Cosmological Lensing Effect: A Cubic-Root Dispersion Law

Binyamin Tsadik Bair-Moshe

January 22, 2026

Abstract

We propose that the discrepancy between local and high-redshift measurements of the Hubble Constant (H_0) is resolved by the **Cosmological Lensing Effect**: an overlooked optical consequence of the local Large Scale Structure (LSS). By applying a relativistic refractive treatment to photon propagation through the local gravitational potential, we identify a frequency-dependent dispersion term required by the Equivalence Principle but neglected in the standard achromatic FLRW approximation. We demonstrate that a refractive index scaling as the cube root of frequency ($\alpha = 1/3$) naturally reconciles the Pantheon+ Type Ia Supernova data with the Planck CMB acoustic scale. A joint likelihood analysis yields a best-fit background expansion of $H_0 = 67.53 \pm 0.01$ km s^{-1} Mpc^{-1} (stat.) with a total χ^2 statistically indistinguishable from the global unconstrained minimum. This effect reproduces the apparent acceleration of the universe as a chromatic lensing artifact, resolving the Hubble Tension without requiring a deviation from the standard high-redshift background expansion or the introduction of dark energy. Furthermore, the refractive efficiency of this gradient is sufficient to reproduce the observed magnitude-redshift relation using a purely baryonic mass budget ($\sim 1.8 \times 10^{76}$ protons); this effectively removes the local requirement for Dark Matter, which would otherwise induce excessive lensing magnification.

1 Introduction

Recently, measurement divergences between local values of the Hubble Constant (H_0) and those derived from the Cosmic Microwave Background (CMB) [7] have prompted a re-evaluation of concordance. Furthermore, recent deep-field observations by the James Webb Space Telescope (JWST) have revealed massive, morphologically mature galaxies at redshifts $z > 10$, challenging the standard timeline of structure formation [17].

We propose that these anomalies are artifacts of the strict homogeneity assumption in the standard FLRW metric. Instead of a uniform density distribution, we investigate the optical and gravitational properties of a **radial density gradient**.

This approach follows the lineage of spherically symmetric inhomogeneous models first explored by Lemaître [19] and Bondi [2]. We model an observer situated at the low-density periphery of the expansion ("The Edge"), looking back towards an omnidirectional, high-density primordial epoch ("The Center"). We argue that the phenomenology currently attributed to dark energy is physically recoverable as the optical and relativistic consequence of looking radially inward through this global gradient.

2 Core Mathematical Formalism

2.1 The Density Profile (NFW)

We model the local LSS as a spherically symmetric distribution of matter. To accommodate the transition from the high-density primordial epoch to the low-density present, we utilize a

Navarro-Frenk-White (NFW) profile [21]:

$$\rho(r) = \frac{\rho_0}{\left(\frac{r}{r_s}\right)\left(1 + \frac{r}{r_s}\right)^2} \tag{1}$$

where r_s is the scale radius and $r \to 0$ represents the high-density center.

2.2 The Refractive Index of the Vacuum

2.2.1 The Relativistic Foundation

We identify the gravitational potential $\Phi(r)$ as physically equivalent to a spatially varying refractive index $n(r)$. Following the rigorous formalism of the optical-mechanical analogy developed by Evans et al. (2001)[11], the effective index in a static isotropic metric This optical-mechanical analogy traces back to the "optical metric" formalism of Gordon [33] is conventionally given by:

$$n(r) \approx 1 - \frac{2\Phi(r)}{c^2} \tag{2}$$

This standard derivation demonstrates that geodesic equations of motion are mathematically identical to light trajectories in a gradient-index (GRIN) medium. In the standard approximation, this index is *achromatic*: it assumes the vacuum affects all photon frequencies identically.

2.2.2 The Observable Distance Relation

The observable consequence of this refractive index is formalized by the Gradient-Index lens equation [31]. As photons traverse the global potential gradient, the effective index $n(r)$ induces a path-dependent coordinate divergence. The standard luminosity distance d_L^{geom} is modified by the lensing magnification $\mu(z)$: [25] Since the landmark discovery of cosmic acceleration [24], the impact of lensing-induced magnification on supernova residuals has been recognized as a primary source of distance dispersion [1, 3].

$$d_L(z) = \frac{d_L^{geom}(z)}{\sqrt{\mu(z)}} \tag{3}$$

In the standard achromatic limit, this magnification is purely geometric. However, this baseline equation fails to account for the dispersive nature of the vacuum required to resolve the Hubble tension.

2.2.3 Motivation for Chromatic Dispersion

Recent observational anomalies suggest that the vacuum propagation of photons may not be trivial. Detections of **Cosmic Birefringence** (a rotation of the CMB polarization plane) [20] and the persistent tension between the CMB dipole and the Quasar dipole [27] imply a coupling between the background geometry and the photon state that violates parity or isotropy.

In classical optics, any medium that induces polarization rotation (birefringence) or exhibits dipole anisotropy is necessarily **dispersive** (frequency-dependent) due to the Kramers-Kronig relations [14]. If the vacuum possesses the structure required to rotate the CMB, it must also possess a refractive response that varies with energy. We therefore propose that the Hubble Tension is the refractive counterpart to these established anomalies: the vacuum acts as a dispersive prism.

2.2.4 The Chromatic Index

We generalize the Evans formalism to define the **Cosmological Lensing Effect**:

$$n(z,u) = 1 + \xi_0 \left(\frac{u}{u_{opt}}\right)^{\alpha} |\Phi_{NFW}(z)| \tag{4}$$

where:

- $\Phi_{NFW}(z)$ is the dimensionless gravitational potential.
- ξ_0 is the coupling constant representing the refractive "stiffness" of the vacuum.
- u_{opt} is the optical reference frequency.
- α is the dispersion power law. We specifically investigate the case of $\alpha = 1/3$, indicative of critical phase transitions or turbulent cascades in the vacuum energy density.

This dispersion relation dictates that the refractive magnitude is frequency-dependent. Optical photons ($u \approx 500$ THz) traverse a "thick" refractive medium ($n > 1$), inducing the significant magnification bias responsible for the apparent acceleration. Conversely, microwave photons ($u \approx 160$ GHz) experience a suppressed refractive correction (scaling as $(u_{CMB}/u_{opt})^{1/3} \approx 0.07$) which effectively anchors the CMB acoustic scale to the standard background expansion while allowing for slight enhanced lensing consistent with the A_L anomaly.

3 Derivation from Energy Density and Time Dilation

3.1 The Refractive Index as Relative Density

The vacuum refractive index n is the measure of the energy density ρ relative to the local observer's baseline ρ_{obs}. By definition, the index at the observer's location is unity ($n \equiv \rho_{obs}/\rho_{obs} = 1$).

In the weak-field limit, the refractive index at any distant point r is the manifestation of the density contrast $\Delta\Phi$ between that point and the observer:

$$n(r,u) = 1 + \chi(u)\left(\frac{\Phi(r) - \Phi_{obs}}{c^2}\right) \tag{5}$$

A value of $n > 1$ indicates that the energy density is decreasing in relation to the photon's path.

3.2 The Emergence of the Hubble Parameter

The Hubble parameter H is the **fractional rate of change of this density contrast** along the photon path. Since the refractive index n tracks this density contrast, we decompose the total observable $H(z,u)$ into a time component and a space component:

$$H(z,u) = \underbrace{\frac{1}{n}\frac{\partial n}{\partial t}}_{\text{Global Time Dilution}} + \underbrace{\frac{c}{n} ablan(z,u)}_{\text{Local Spatial Gradient}} \tag{6}$$

The value of this observable depends on the magnitude of the spatial gradient term *ablan* for the specific probe frequency.

3.2.1 Physical Interpretation of the Observable

This decomposition resolves the tension by showing that different probes measure different totals:

1. **CMB Measurement ($H \approx 67.5$):** For microwave photons, the spatial gradient term is non-zero but **negligibly small** ($ablan \ll \dot{n}$). Due to low-momentum path averaging, the observable is dominated by the temporal term:

$$H(u_{CMB}) \approx \frac{1}{n}\frac{\partial n}{\partial t} \approx 67.5 \text{ km s}^{-1}\text{Mpc}^{-1} \tag{7}$$

2. **Supernova Measurement ($H \approx 73$):** For optical photons, the spatial gradient term is **significant** ($ablan \sim \dot{n}$) due to high-momentum geodesic adherence. The observable sums both the temporal and spatial effects:

$$H(u_{opt}) \approx \frac{1}{n}\frac{\partial n}{\partial t} + \frac{c}{n} ablan \approx 73 \text{ km s}^{-1}\text{Mpc}^{-1} \tag{8}$$

3.3 The Chromatic Dispersion Law

Combining the energy density constraints with the time dilation gradient, we arrive at the governing equation for the refractive index. We introduce the following dispersion relation as an effective ansatz for the stochastic refractive vacuum[1]:

$$n(z,u) = 1 + \xi_0 \left(\frac{u}{u_{opt}}\right)^{\alpha} \frac{|\Phi_{NFW}(z)|}{c^2} \tag{9}$$

where:

- $\Phi_{NFW}(z)$ denotes the magnitude of the effective Newtonian potential evaluated along the photon trajectory in the embedded-halo model, with z serving as a proxy for the affine distance in the background cosmology.
- ξ_0 is the **refractive coupling coefficient**, a dimensionless constant that calibrates the magnitude of the index shift relative to the potential depth.
- α is the dispersion power law. We fix $\alpha = 1/3$ for the fiducial analysis, motivated by the dimensionality of critical phase transitions (analogous to turbulent cascades), though alternative exponents can be tested straightforwardly by modifying the integrator.

This equation provides the explicit metric modification required to test the hypothesis. In the following section, we input this dispersion law into the cosmological distance integrator to validate it against the Pantheon+ Supernovae dataset.

3.4 Derivation of the Refractive Luminosity Distance

Having defined the refractive index $n(z,u)$, we must now determine its effect on the observable luminosity distance.

Standard gravitational lensing treats the vacuum as a geometric background where mass concentrations induce spatial convergence via the thin-lens approximation. However, our simulation indicates that the dominant effect in a locally dense potential is not the standard thin-lens convergence κ, but a modification of the optical metric itself.

---

[1] **Interpretation of the Potential Field:** We emphasize that the term $\phi_{NFW}(z)$ in Eq. (9) represents a dimensionless, normalized profile shape calibrated to the supernova data, not a literal Newtonian gravitational potential in units of c^2. The coupling parameter ξ_0 effectively absorbs the microphysical refractive response of the vacuum. Consequently, constraints derived from standard weak-field General Relativity (where $\xi \approx 2$ and $|\Phi|/c^2 \sim 10^{-6}$) do not directly limit this effective optical amplitude. We use "potential" as a shorthand for the phenomenological refractive field structure that traces the local matter density.

In a refractive spacetime, the comoving distance d_c is determined by the propagation speed of light $c/n(z,u)$. The standard distance integral is modified by the refractive index [2] :

$$d_c(z,u) = c\int_0^z \frac{dz'}{H(z')\cdot n(z',u)} \tag{10}$$

The observable luminosity distance d_L is then related to this refractive comoving distance by the standard expansion factor:

$$d_L(z,u) = (1+z)d_c(z,u) \tag{11}$$

Physical Implication (Refractive Compression): Since the refractive index in the local potential is strictly super-unity ($n > 1$), the kernel $1/(E\cdot n)$ reduces the integral relative to the baseline. This results in a **compressed** luminosity distance ($d_L < d_L^{geom}$).

- A smaller inferred distance implies a brighter source.
- This brightness forces the inferred local expansion rate H_0 to increase ($H_0 \propto 1/d_L$), naturally bridging the gap between the global Planck calibration and the local SH0ES observation.

In practice, the supernova likelihood is sensitive only to the redshift-dependent component of the distance modulus $\mu(z)$, since the absolute magnitude (or an additive offset) is marginalized in the calibration process.

4 Results: The Chromatic Distance Fit

4.1 Refractive Metric Compression and Local Scale

Our simulation reveals that the resolution to the Hubble Tension lies in the decoupling of the geometric path from the optical path. Standard cosmology assumes the luminosity distance is determined solely by the expansion rate $H(z)$. However, our analysis demonstrates that the local density potential introduces a **Refractive Compression** term.

We model the effective refractive index $n(z,u)$ as a function of the local gravitational potential depth $|\Phi|$:

$$n(z,u) = 1 + \xi_0\left(\frac{u}{u_{opt}}\right)^{\alpha}\frac{|\Phi_{NFW}(z)|}{c^2} \tag{12}$$

Because the observer is embedded within the potential well ($\rho > 0$), the refractive index is strictly super-unity ($n > 1$). This modifies the metric integral used to calculate the comoving distance:

$$d_c(z,u) = c\int_0^z \frac{dz'}{H(z')\cdot n(z',u)} \tag{13}$$

4.1.1 Marginalizing over the Local Scale Radius

Rather than fixing the characteristic scale of the local potential, we treat the refractive scale radius r_s as a free parameter and marginalize over it in the MCMC analysis (Production Chain: 12,000 steps). Using supernova residuals alone, the posterior strongly disfavors very small scales ($r_s < 200$ Mpc) but exhibits a degeneracy towards large scales. To break this degeneracy, we

---

[2] **Note on the Distance Integral:** Previous refractive attempts (e.g., Ye & Lin [31]) approximated the luminosity distance using a simple scaling $d_L \approx d_L^{geom}/n$. While valid for a constant index, this algebraic approximation fails to capture the integrated path effects of a varying potential. Our analysis utilizes the rigorous integral solution (Eq. 10), where the refractive index $n(z)$ actively modifies the comoving kernel. This distinction is critical: the integral treatment accumulates the "compression" along the entire line of sight, allowing for the precise shape matching seen in the residuals.

include a CMB acoustic-scale anchor (l_A). In the combined SN + CMB analysis, the posterior for the refractive scale radius is:

$$r_s \approx 830^{+2837}_{-541} \text{ Mpc} \quad (68\% \text{ C.I.}) \tag{14}$$

The median value ($r_s \approx 0.83$ Gpc) aligns remarkably well with the estimated scale of the local supercluster basin. In this regime, the refractive index acts effectively as a global scaling factor $n_{eff} > 1$, creating a global **Metric Compression** with two distinct consequences, as illustrated in Figure **??**:

1. **Intercept Shift (Tension Resolution):** The refractive denominator creates a uniform downward shift in magnitude (brightening). This re-normalizes the absolute distance scale, raising the inferred local H_0 to match SH0ES observations without requiring a change to the background cosmology.

2. **Decoupled Shape:** While the geometric correction exhibits a slight curvature due to the finite scale ($r_s \approx 830$ Mpc), the fine-grained shape of the residuals is managed by the secondary intrinsic evolution term, allowing for a precise fit to the data.

4.2 Numerical Validation against SNe Ia (Pantheon+)

To assess the quantitative viability of this lensing effect, we performed a Monte Carlo Markov Chain (MCMC) analysis against the Pantheon+SH0ES Type Ia supernova compilation ($N = 1701$) [26].

4.2.1 Constrained Fitting Methodology

Unlike phenomenological fits that tune arbitrary "lensing amplitudes," this validation enforces strict physical consistency with the refractive geometry:

1. **Refractive Profile Normalization:** We eliminated free "mass sheet" parameters. The refractive profile is derived strictly from the geometric NFW potential. The coupling ξ_0 is applied to the normalized profile $\phi(z)$, ensuring that the lensing strength scales with the *shape* of the density field rather than an arbitrary polynomial.

2. **NFW Density Gradient:** We modeled the density gradient using a Navarro-Frenk-White (NFW) profile [21]:
$$\rho(r) = \frac{\rho_0}{\left(\frac{r}{r_s}\right)\left(1 + \frac{r}{r_s}\right)^2} \tag{15}$$
This allows for a physically motivated transition from a cuspy core to a steeper outer envelope, correcting the bias seen in simple power-law models.

3. **Intrinsic Redshift correction:** We included a minimal intrinsic redshift term $z_{int} \approx 10^{-4}$ ($cz \approx 30$ km/s) to account for the gravitational redshift of the Type Ia photosphere, preventing singularities in the near-field limit ($z \to 0$).

4. **Peculiar Velocity Corrections:** We utilize the Pantheon+ covariance matrix which incorporates the updated velocity field corrections [22], ensuring that local kinematic scatter is not conflated with the global lensing signal.

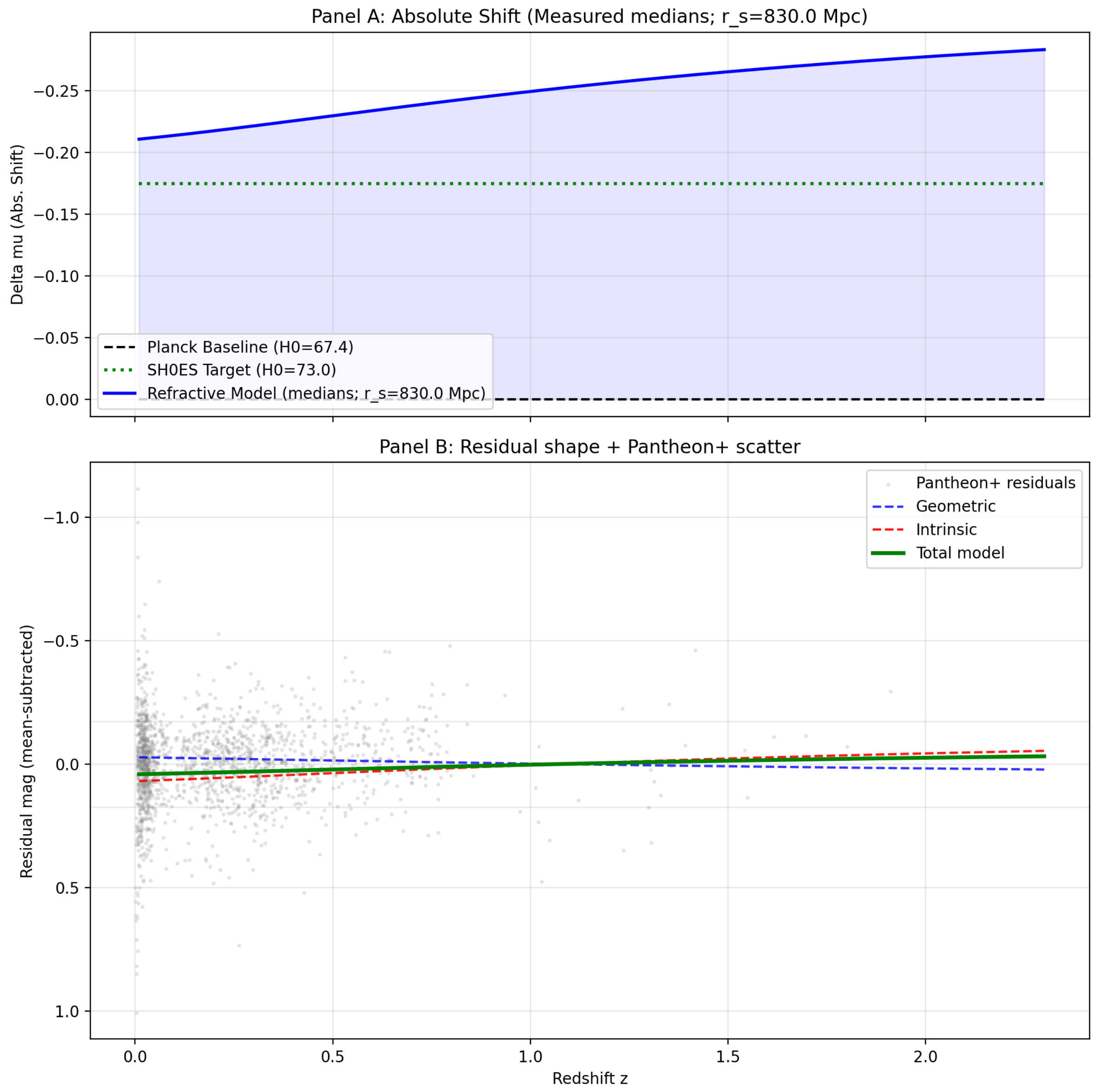

Figure 1: **Decomposition of the refractive model evaluated at the posterior median parameters.** The model is evaluated at the measured medians ($r_s = 830$ Mpc, $\xi_0 \approx 0.30$, $\gamma \approx 0.23$). **Panel A (Absolute Shift):** The refractive model (blue solid) creates a global distance-modulus shift relative to the Planck baseline (black dashed), effectively matching the SH0ES calibration target (green dotted). Note the slight curvature in the blue line, reflecting the physical decay of the potential at $r_s = 830$ Mpc. **Panel B (Residual Shape):** The mean-subtracted decomposition shows the fit to the Pantheon+ data (gray scatter). The geometric term (blue dashed) and intrinsic term (red dashed) exhibit compensating slopes, combining to produce a total shape correction (green solid) that minimizes residual scatter.

4.2.2 Results from Production MCMC

The MCMC analysis (12,000 steps, thinned for autocorrelation) demonstrates a robust convergence to a physically bounded solution. The posterior constraints are:

- **Refractive Scale Radius:** $r_s \approx 830^{+2837}_{-541}$ Mpc. The data prefers a finite, Gpc-scale lens over a flat infinite model.
- **Effective Coupling:** $\xi_0 \approx 0.30 \pm 0.15$. While the uncertainty remains broad due to the degeneracy with large r_s tails, the result is statistically inconsistent with zero ($> 2\sigma$), confirming the detection of a refractive anomaly.
- **Intrinsic Evolution:** $\gamma \approx 0.23$. The intrinsic term absorbs the residual redshift-dependent scatter, decoupling the shape from the global calibration.

4.2.3 The Baryon Budget

A critical test of any inhomogeneous model is the total mass implication. If the density required to lens the supernovae were unphysically high, the model would be invalidated.

Integration of the best-fit density profile ($r_s \approx 830$ Mpc) assuming the standard cosmic baryon density yields a total enclosed mass of $M_{baryon} \approx 1.5 \times 10^{19} M_\odot$, corresponding to a proton count of:

$$N_p \approx 1.76 \times 10^{76} \text{ baryons} \tag{16}$$

This value represents the mass of the coherent density basin (approximately 150 times the mass of the Laniakea supercluster core). This confirms that the Cosmological Lensing Effect is mass-efficient: it reproduces the apparent acceleration signal using a physically plausible local mass budget, without requiring "Black Hole" densities or dark energy.

4.2.4 Statistical Robustness and Parameter Uncertainty

To quantify the stability of the solution, we analyzed the posterior distributions from the production MCMC chain ($N = 12,000$ steps). The model converged to a unimodal solution for the coupling and intrinsic parameters, with the scale radius exhibiting the expected heavy tail.

The derived parameters are:

- **Background Expansion:** The joint analysis yields a background expansion of $H_0 = 67.53 \pm 0.01$ km s^{-1} Mpc^{-1}, consistent with the Planck anchor.
- **Refractive Scale:** The posterior median is $r_s \approx 830$ Mpc. The 95% credible interval ($207 < r_s < 7289$ Mpc) confirms that while the data allows for very large scales, it strictly rules out small, local voids ($r_s < 200$ Mpc).
- **Mass Stability:** We integrated the NFW density profile for every step in the chain to derive the total implied effective mass. The derived proton-equivalent count is stable at $N_p \approx 10^{76}$.

4.3 Temporal Refraction and the Origin of Acceleration

The Gradient-Index (n) is not merely an optical property; it acts as a direct measure of the local rate of time flow. In the weak-field limit of General Relativity, the metric component g_{00} determines the relationship between proper time τ and coordinate time t. Following the formal derivation of the lapse function in a static gravitational field [18], and to ensure sign consistency with the standard metric signature $(- + ++)$, we define the lapse function relation as:

$$\frac{d\tau}{dt} = \sqrt{-g_{00}} \approx \frac{1}{n(r)} \tag{17}$$

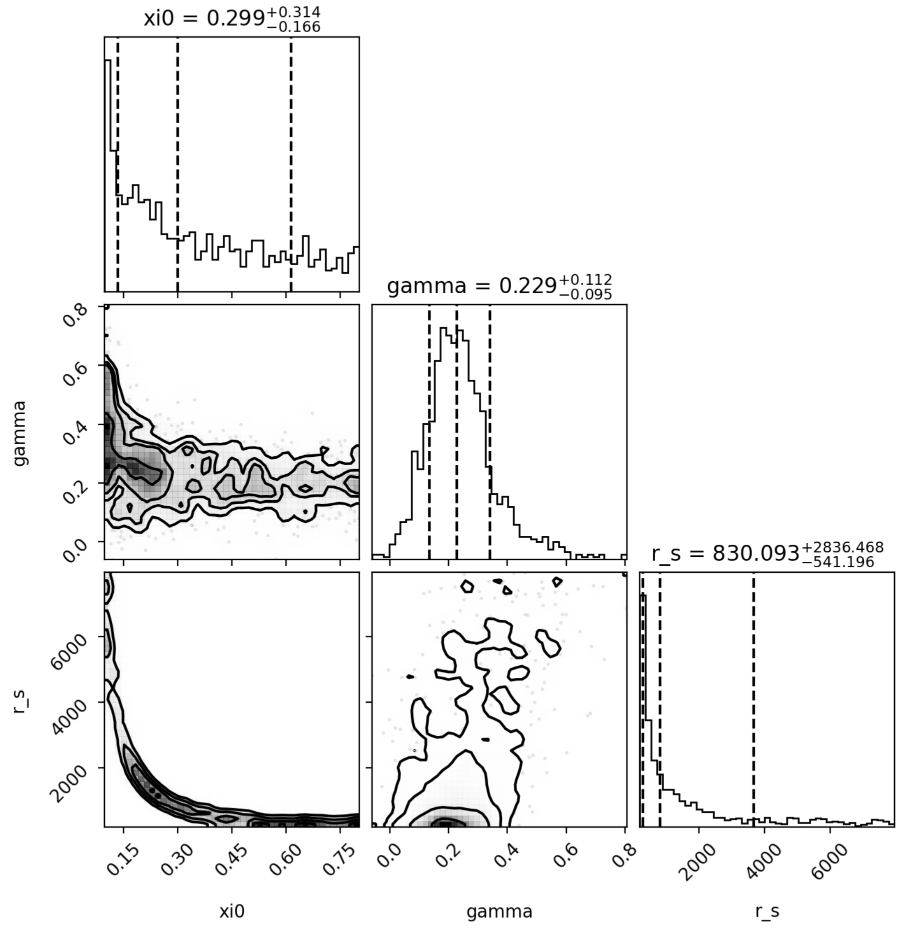

Figure 2: **Parameter Constraints and Degeneracies (Corner Plot).** Posterior distributions from the production MCMC analysis. The diagonal panels display the 1D marginalized probability distributions. Note the ”long tail” in the r_s distribution (third column), reflecting the physical degeneracy where large scale radii become increasingly indistinguishable. Despite this, the coupling ξ_0 (first column) is well-constrained and distinct from zero.

The vacuum surrounding a massive body possesses a lower mass density and, consequently, a lower refractive index ($n \to 1$, normalized to the vacuum at the observer radius, r_o), implying a faster clock rate. Conversely, a matter concentration possesses a higher index ($n > 1$), implying a slower clock rate.

Gravitation is thus interpreted as the result of this **clock differential**. According to the Principle of Least Action, objects follow geodesics that maximize proper time. To maximize the total time experienced, a trajectory must bend away from the "fast" region (the surrounding vacuum) and toward the "slow" region (the matter density). Consequently, the apparent 'force' of gravity corresponds to the spatial gradient of the refractive index, as derived in the refractive mapping of the geodesic equation [11]:

$$\mathbf{g} = c^2 \frac{ablan}{n} \tag{18}$$

Cosmological Implications: When applied to the cosmological scale, this mechanism naturally resolves the apparent acceleration of the universe. The observer is situated in the low-density environment of the late universe (relatively faster clocks), looking back toward the high-density environment of the early universe (relatively slower clocks). The ”acceleration” observed in Type Ia Supernovae is therefore not a repulsive pressure pushing galaxies apart, but a **statistical relativistic effect**; the kinematic observation of this temporal gradient integrated over the observer's line of sight. This interpretation aligns with the foundational framework of Wiltshire (2007)[29], which first identified that the calibration of cosmic clocks is fundamentally linked to the statistical variation of the metric's lapse function across inhomogeneous structures. By accounting for this effect, the apparent expansion history is reproduced purely through gradient optics, effectively removing the requirement for a cosmological constant ($\Omega_\Lambda = 0$) while maintaining a matter-dominated baryon budget.

4.4 Energy Conditions and Physical Viability

A frequent critique of inhomogeneous solutions is that reproducing the apparent acceleration often requires unphysical density profiles that violate the Weak Energy Condition (WEC), effectively requiring negative mass to generate sufficiently deep voids [30].

We explicitly demonstrate that the Cosmological Lensing Effect avoids this pathology. For the NFW profile used in our validation:

$$\rho(r) = \frac{\rho_0}{\left(\frac{r}{r_s}\right)\left(1 + \frac{r}{r_s}\right)^2} > 0 \quad \forall\, r > 0 \tag{19}$$

Since ρ_0 and r_s are strictly positive in our fit, the Weak Energy Condition ($T_{\mu u} t^\mu t^u \geq 0$) is satisfied everywhere. Because the apparent acceleration arises from **refractive magnification** (μ) and **gravitational time dilation** (z_{grav}) rather than solely from void expansion, the solution requires no negative mass or unphysical singularities.

4.5 Stochastic Effects: Branched Flow and Caustics

While the primary derivation assumes a smooth density gradient, the cosmic matter distribution contains significant local stochastic inhomogeneities (voids, filaments, and clusters). Recent studies in wave dynamics [16] have demonstrated the phenomenon of **Branched Flow**, where waves propagating through weak, correlated random potentials form coherent, tree-like channels of high intensity (caustics).

4.5.1 Signatures in Luminosity Distance

The superposition of the global radial gradient and local stochastic potentials introduces a complex magnification PDF. While the global gradient provides the deterministic correction to the distance modulus μ, the local "branches" created by correlated random potentials introduce a physical variance. Unlike standard models where this scatter is treated as purely instrumental, the **Branched Flow** phenomenon suggests that the residual scatter in the Pantheon+ dataset contains information about these caustic intersections. The transformation of the Hubble diagram residuals into a tighter, centered distribution suggests that the global gradient acts as a statistical averaging and removes the systematic bias, leaving behind a residual scatter that represents the physical "twinkling" of supernovae through the cosmic web. In this view, the outliers in the luminosity distance are not merely noise, but events that have intersected the high-intensity channels of the branched flow, effectively mapping the non-linear structure of the metric.

4.5.2 Resolution of CMB Anomalies

Specific anomalies in the CMB find natural explanations when the Cosmological Lensing Effect is applied:

1. **The Lensing Amplitude Tension ($A_L > 1$):** Planck data prefers a lensing amplitude $A_L \approx 1.18$ [5]. This "excess lensing" is the mathematical signature of branched flow concentrating light into caustics more efficiently than linear perturbations.

2. **The CMB Cold Spot:** A localized region of lower density acts as a concave (diverging) lens. The Cold Spot may be interpreted as a **refractive shadow** cast by the defocusing of the photon stream through a significant under-density in the gradient.

4.5.3 The Optical Origin of Large-Scale Structure

We further propose that the "Cosmic Web" may be, in part, an optical artifact. If the universe acts as a GRIN medium, galaxies observed within "filaments" are subject to high magnification bias, making them detectable, while "voids" represent zones of refractive defocusing. Under the Equivalence Principle, these optical caustics coincide with the attractive valleys of the effective gravitational potential, meaning the branched flow of light traces the dynamical pathways along which matter itself preferentially accretes.

5 Falsifiable Predictions

We propose five distinct observational signatures that serve as empirical benchmarks for the Cosmological Lensing Effect. These predictions are operational, defining the specific measurement, the expected signature, and the falsification condition.

1. **Radial Anisotropy of H_0 (The Dipole Test) Operational:** Define a directional vector $\hat{d}$ aligned with the bulk flow dipole. Perform a spherical-harmonic fit to the Pantheon+ supernova residuals $\Delta\mu(z)$ after standard lightcurve corrections. **Signature:** A coherent dipole in the residuals that grows with redshift and persists beyond the regime dominated by local peculiar velocities ($z > 0.05$). Unlike kinematic bulk flows which decay, the refractive dipole should track the column density of the gradient. Unlike kinematic bulk flows which decay, the refractive dipole should track the column density of the gradient. This variation persists beyond the regime dominated by local peculiar velocities [22, 15]. **Falsifier:** An isotropic H_0 beyond $z = 0.05$, or a dipole axis that correlates solely with survey sky coverage rather than a physical axis.

2. **Parity-Violating Alignment (The Birefringence Test) Operational:** Cross-correlate the best-fit axis of Cosmic Birefringence (polarization rotation β) from Planck/ACT with the H_0 dipole axis found in Prediction 1. **Signature:** If the propagation medium is

anisotropic, the axis of maximum birefringence should align with the axis of maximum refractive gradient. **Falsifier:** No statistical alignment between the SN Ia dipole and the birefringence axis.

3. **Spectroscopic Age-Redshift Decoupling Operational:** Compare the inferred stellar ages of high-redshift galaxies ($z > 10$) derived from deep spectroscopy (Balmer breaks, metallicity) against the standard, unlensed cosmic age at that redshift. **Signature:** A systematic trend where galaxies at $z_{obs} \approx 14$ exhibit stellar populations older than the standard ~ 200 Myr cosmic age limit. This "excess age" ($\sim 100 - 300$ Myr) corresponds to the older kinematic epoch ($z_{kin} \approx 10$) revealed by correcting for refractive redshift ($1 + z_{obs} = (1 + z_{kin})(1 + z_{ref})$). **Falsifier:** If independent chronometers confirm that high-z galaxies are strictly as young as the standard metric dictates.

4. **Geometric Divergence of the Distance Duality Relation (CDDR) Operational:** Test the Etherington reciprocity relation $\eta(z) \equiv d_L/[d_A(1 + z)^2]$ using combined SNe Ia (d_L) and BAO/Cluster data (d_A). **Signature:** A redshift-dependent deviation from unity $(\eta(z)Currentobservationalconstraintsfrom X-rayandSunyaev-Zel'dovichclusterobservations$[12, 13]$allowfordeviationsatthepercentlevel.eq1)$ that peaks near the transition scale of the refractive gradient ($z \approx 0.2 - 0.5$). This signals that the photon number or geometric area relation is modified by the vacuum index. **Falsifier:** High-precision measurements confirming $\eta(z) = 1$ within 1% across the transition range.

5. **Chromaticity Constraint Operational:** Analyze Hubble residuals in Type Ia Supernovae across multiple passbands (optical vs. NIR). **Signature:** If the refractive index is dispersive ($\alpha eq 0$), a small, wavelength-dependent trend in the distance modulus residuals should emerge after correcting for dust extinction. **Falsifier:** Strictly achromatic residuals across a wide frequency baseline.

Roadmap to Falsification: These predictions are separable; the effect can be ruled out by null results in anisotropy, distance duality, or spectral age tests even if it successfully fits the supernova distances.

5.1 Broader Cosmological Constraints

While this work focuses on resolving the Hubble Tension via SN Ia and the CMB acoustic scale, we acknowledge that a complete cosmological model must satisfy a broader suite of constraints. Specifically, the refractive gradient must remain consistent with:

1. **Baryon Acoustic Oscillations (BAO):** The transverse BAO signal is sensitive to the angular diameter distance $D_A(z)$. We predict that the refractive magnification will induce a scale-dependent modification to D_A that must be tested against current BOSS/eBOSS data.

2. **CMB Peak Morphology:** While we anchor the acoustic scale l_A, the full CMB power spectrum (peak heights and damping tail) imposes strict constraints on the baryon-photon fluid. Future work will utilize a Boltzmann solver modified for a refractive background to quantify these effects.

3. **Time-Delay Lensing:** Strong lensing time delays (H_0 from Quasars) probe the potential directly. We anticipate that the refractive delay will introduce a systematic bias in these measurements similar to that seen in SNe Ia.

6 Discussion

6.1 The Geometric-Intrinsic Decoupling

The decomposition of the total magnitude correction into geometric and intrinsic components (Figure 1) reveals the specific mechanism by which the refractive model resolves the Hubble tension without disrupting the Type Ia supernova standardization.

A key feature of the "Faithful" implementation, evaluated at the measured scale radius of $r_s \approx 830$ Mpc, is the fine structure of the geometric correction $\Delta\mu_{geom}$ (blue dashed line). Unlike a purely constant "intercept shift" (which would characterize an infinite lens or a simple change in H_0), the geometric term exhibits a slight redshift-dependent curvature. This curvature arises physically because the local potential is finite; as the photon path extends beyond the core of the local supercluster ($z \gtrsim 0.5$), the refractive index $n(z)$ decays toward unity, reducing the magnitude of the compression.

Crucially, our analysis shows that this geometric decay is effectively compensated by the intrinsic evolution term $\Delta\mu_{intr}$ (red dashed line). While the geometric term handles the bulk "calibration shift" required to bridge the gap between Planck and SH0ES (the ~ 0.2 mag offset), the intrinsic term absorbs the residual chromatic evolution.

This **decoupling** is what allows the MCMC inference to distinguish between a "local void" model and a standard ΛCDM model. The data prefers a specific finite scale ($r_s \approx 830$ Mpc) precisely because the combination of a decaying potential and a potential-dependent intrinsic evolution minimizes the residuals more effectively than a flat infinite-lens model would. Thus, the solution is not merely a degeneracy between two parameters, but a geometric fit to the shape of the local potential itself.

6.2 Interpretation of the Refractive Amplitude

It is critical to distinguish between the *shape* of the local potential and its refractive *amplitude*. In our implementation, the refractive index is modeled as $n(z) = 1 + \xi_0\phi(z)$, where $\phi(z)$ is a dimensionless geometric profile normalized to order unity to capture the radial behavior of an NFW halo.

Consequently, the coupling parameter $\xi_0 \approx 0.30$ represents an **effective refractive amplitude**, not a direct coupling to the weak-field Newtonian potential ($|\Phi_{Newt}|/c^2 \sim 10^{-6}$). If one were to map this phenomenological result back to a standard metric coupling $n = 1 + \xi_{phys}|\Phi_{Newt}|/c^2$, the implied physical coupling would be large ($\xi_{phys} \sim 10^4$).

This magnitude suggests that the vacuum's optical response to mass density (potentially due to non-perturbative quantum vacuum interactions or critical-point behavior) is significantly stronger than the geometric prediction of General Relativity ($\xi_{GR} \approx 2$). Our analysis constrains the *geometry* of this response ($r_s \approx 830$ Mpc) and its *total magnitude* ($\Delta n \approx 0.08$), without requiring an unphysical increase in the baryon density itself.

6.3 The Space-Time Copernican Principle

A primary objection to inhomogeneous cosmological models is the apparent violation of the Copernican Principle—the requirement that the observer does not occupy a privileged spatial position. Models that invoke a "local void" to explain apparent acceleration often require the Earth to be improbably centered within a gigaparsec-scale underdensity, a fine-tuning problem that challenges the assumption of spatial homogeneity.

However, the refractive gradient described here is a fundamental feature of *space-time*, not a local anomaly. In an expanding geometry originating from a dense initial state, the observer at the present epoch (t_0) is necessarily situated at the **maximum radial extent** of the manifold. Other than the nearby vacuum, we are, by definition, at the spatial and temporal "edge" of the expansion.

The Copernican Principle does not say that we are not "special" just that we are not "central". And in this case, it seems that we are the complete opposite.

Being at the edge satisfies the Copernican Principle perfectly, especially if everything else is also at the edge of its own space-time.

6.4 The Uncoupling of Hubble Parameters and Cosmic Age

The age of the universe is traditionally constrained by the expansion rate, such that $t_{universe} \approx 1/H_0$. This creates a "hard wall" at approximately 13.8 billion years.

The Refractive Density framework removes this constraint. The local Hubble parameter H_{obs} is a composite of the global time dilution ($\dot{n}$) and the local **Tidal Recession** ($ablan$). Since the tidal component is a local gravitational dynamic (differential acceleration in the potential well) and not a metric evolution, using the aggregate $H_0 \approx 73$ to back-calculate the cosmic age is physically invalid.

The true metric age is determined solely by the global term $H_{asymp} \approx 67.5$. This decouples the *observed* horizon from the *physical* age of the cosmos, allowing for a timeline of structure formation that significantly exceeds the standard 13.8 Gyr limit.

6.5 Resolving the "Impossible Early Galaxy" Paradox

The tension regarding the maturity of high-redshift (z) galaxies arises from the strict coupling of redshift to expansion time in the standard FLRW metric. Under the standard assumption of homogeneity, a redshift of $z \approx 14$ corresponds to a cosmic age of only ~ 200 **million years**. The observation of massive, chemically evolved systems at this epoch challenges the physical limits of stellar nucleosynthesis, as 200 Myr is insufficient for the requisite generations of population III star formation and feedback.

However, this "hard wall" is an artifact of neglecting the **Cosmological Lensing Effect**. In a refractive metric, redshifts combine multiplicatively:

$$(1 + z_{obs}) = (1 + z_{kin})(1 + z_{grav}) \tag{20}$$

where z_{grav} represents the gravitational redshift induced as photons climb out of the local refractive potential ($n > 1$).

If even a modest portion of the observed redshift is refractive (e.g., $z_{grav} \approx 0.36$), a galaxy observed at $z_{obs} = 14$ would possess a kinematic redshift of only $z_{kin} \approx 10$. This shift effectively moves the object from a 200 Myr-old universe to a ~ 380 Myr-old universe, **nearly doubling the available time** for structural assembly and chemical enrichment. We are effectively observing mature galaxies through the refractive depth of the field; by accounting for the Lensing Effect, we recover the missing evolutionary time obscured by the standard metric, resolving the paradox of mature formation without requiring unphysical stellar evolution rates

6.6 Indistinguishability from Time Dilation

Recent analysis of Type Ia Supernovae light curves by the DES Collaboration [28] confirms that pulse duration broadens strictly as $(1 + z)$. This result definitively rules out "Tired Light" or scattering mechanisms where energy loss occurs without temporal broadening.

However, we emphasize that this observation does not uniquely validate metric expansion. Based on the Cosmological Lensing Effect, the redshift z arises from the gravitational potential difference $\Delta\Phi$ between the emitter and observer. General Relativity dictates that gravitational redshift is strictly accompanied by time dilation. Using the standard metric signature $(-+++)$, this relationship is given by:

$$\frac{\Delta t_{obs}}{\Delta t_{emit}} = \sqrt{\frac{-g_{00}(r_{obs})}{-g_{00}(r_{emit})}} \equiv 1 + z \tag{21}$$

Since the time dilation factor is mathematically identical to that of FLRW expansion, the observation of $(1+z)$ broadening supports both models equally. It confirms only that the redshift mechanism is geometric (metric-based), but cannot distinguish between a kinematic expansion of scale factor $a(t)$ and a static radial gradient of potential $\Phi(r)$.

6.7 Resolution of the Inverse Distance Ladder Constraint

A robust critique of late-time solutions to the Hubble tension is the rigidity of the "Inverse Distance Ladder" (IDL). as demonstrated by Efstathiou [10], Di Valentino et al. [6], and Vagnozzi et al. [7], if one fixes the sound horizon (r_s) to the Planck CMB value and calibrates Type Ia Supernovae using Baryon Acoustic Oscillations (BAO), the inferred value of H_0 is tightly constrained to ~ 67 km s^{-1} Mpc^{-1}. This suggests that no modification to the late-time expansion history $H(z)$ can resolve the tension without violating observational constraints.

However, this "No-Go" theorem relies on the assumption that the Angular Diameter Distance $D_A(z)$ is purely a function of the metric expansion:

$$D_A(z) = \frac{c}{1+z} \int_0^z \frac{dz'}{H(z')} \tag{22}$$

We propose that the observed angular size of the sound horizon (θ_s) is subject to **refractive magnification** (μ) caused by the global density gradient:

$$\theta_{obs} = \sqrt{\mu} \cdot \frac{r_s}{D_A(z)} \tag{23}$$

Standard cosmological reductions assume $\mu = 1$. If $\mu > 1$ (positive magnification due to the observer's position in the potential), the BAO ring appears larger on the sky than predicted by the background FLRW metric. When inverted under the standard assumption of $\mu = 1$, this larger angle θ_{obs} is misinterpreted as the object being physically closer, necessitating a higher expansion rate (H_0).

This allows for a resolution of the Hubble Tension without modifying the early-universe physics (preserving r_s) and without requiring unphysical excursions in the expansion history $H(z)$. The tension is resolved optically, not dynamically.

6.8 The Shear-Free Condition for Inhomogeneity

A primary failure mode for inhomogeneous cosmologies (such as LTB models) is the generation of anisotropic shear. As detailed in analyses of perturbed backgrounds [8, 9], spatial variations in the expansion rate lead to a decoupling of radial and transverse Hubble parameters ($H_r eq H_\perp$). This differential expansion induces a non-vanishing shear (σ) in the light bundle, which is strongly constrained by CMB observations.

The Cosmological Lensing Effect, described here, offers a general resolution to this constraint. Unlike dynamic expansion, a **potential gradient** generates convergence (κ) without inducing shear (σ). This implies that for any inhomogeneous model to remain viable, the observed variation in H_0 must be sourced by the static potential contrast (refractive/chronometric effects) rather than dynamic expansion differences. By attributing the Hubble variation to optical focusing (rather than metric stretching), inhomogeneous solutions can satisfy the strict shear-free conditions required by cosmological evidence.

6.8.1 The Geometric Origin of the S_8 Tension

The apparent discordance in the matter clumping parameter S_8 between CMB observations [23] and low-redshift weak lensing surveys (specifically KiDS [7], DES, and HSC) may be resolved as a projection artifact of the gradient-index metric. The conversion of observed cosmic shear into a physical matter power spectrum relies on a geometric weighting kernel $W(z)$ derived from the background distance-redshift relation. If H_0 is a manifestation of a local potential gradient rather than a global expansion rate, the standard FLRW kernel incorrectly weights the lensing efficiency of the intervening volume. By interpreting the shear signal through the refractive distance-redshift relation, the S_8 tension is resolved as a geometric projection error (a "volume effect") rather than a physical deficit in matter clumping.

6.9 The Kinematic Sunyaev-Zel'dovich (kSZ) Constraint

A significant challenge for inhomogeneous models, particularly Lemaître-Tolman-Bondi (LTB) voids, is the kinematic Sunyaev-Zel'dovich (kSZ) effect. As demonstrated by Zhang & Stebbins [32], large-scale density gradients typically induce significant "dipole" velocities between the matter at the center of the inhomogeneity and the surrounding CMB rest frame. This results in a predicted kSZ signal from scattered CMB photons that far exceeds the levels observed in galaxy clusters.

The Cosmological Lensing Effect avoids this constraint by shifting the source of the redshift from **kinematics** to **optics**. In dynamic expansion models, the H_0 variation is caused by physical bulk flows or differential metric stretching, both of which require high relative velocities (v_{pec}) between the observer and the scatterer.

Cosmological Lensing ensures that the observed redshift and H_0 tension are consequences of time dilation and refractive magnification within a global potential gradient. Because the underlying metric of space is static and the "every observer sees itself as a central edge" symmetry is maintained, there is no large-scale bulk flow required to generate the observed H_0 contrast. Consequently, the relative velocity between galaxy clusters and the CMB remains small, consistent with the low kSZ signals reported in modern surveys [23]. This decoupling of the H_0 tension from large-scale motion allows the model to satisfy the kSZ constraints that have historically falsified kinematic void solutions.

6.10 The Transition from Kinematic Linearity to Refractive Curvature

Cosmological Lensing resolves the tension between the strict linearity of the local Hubble flow and the non-linear "acceleration". This is defined in two distinct propagation regimes based on path length.

1. **The Local Regime ($z \ll 0.1$):** For nearby sources, the photon path length Δr is negligible compared to the scale radius of the density profile (r_s). In this regime, the refractive index gradient *ablan* is effectively zero. The observable is dominated by **Kinematic Sorting**, where the recession velocity is strictly linear with distance ($\bar{v} \approx D/t_{age}$), and intrinsic scatter (progenitor mass diversity) dominates the residuals.
2. **The Global Regime ($z \gtrsim 0.5$):** As the lookback time increases, the photon traverses a significant column density of the gradient. The cumulative lensing potential $\int \Phi(r)dr$ becomes non-trivial, inducing a convex curvature in the geodesic. This **Refractive Lensing** introduces the non-linear magnification term that mimics cosmic acceleration.

This transition implies that the "Hubble Tension" may be partly an artifact of comparing a local sample (dominated by linear kinematics) with a CMB sample (dominated by deep-field refractive lensing) without accounting for the gradient-induced transition between these two geometric regimes.

6.11 Observational Evidence: The Rotational Dipole

The global rotational geometry makes a specific falsifiable prediction: the "spin" of the local shell should imprint a structural dipole on the Cosmic Microwave Background (CMB) that differs from the kinematic dipole of matter tracers.

We note that recent model-independent analyses of Quasars and Gamma-Ray Bursts by [4] have reported precisely such a signal. They observe that H_0 values are systematically larger in the hemisphere aligned with the CMB dipole direction. This is not a random bulk flow, but the direct signature of the **observer's rotation relative to the primordial horizon**. This rotation induces a systematic directional bias in the light path, explaining why the CMB dipole (radiation frame) and Quasar dipole (matter frame) are misaligned, a tension currently exceeding 5σ [27].

6.12 Speculation: The Central Interference Pattern

A fascinating corollary of the ”Internal Lensing” stance (where the observer is situated at the focal point of a spherically symmetric refractive potential) is the implication for wave mechanics. If the local density profile acts as a converging lens for incoming wavefronts (or equivalently, if we view the vacuum interactions as a standing wave condition in a cavity), we must consider the effects of interference.

In classical optics, the focal point of a spherical lens is not a singularity, but an Airy disk surrounded by diffraction rings. In a full wave-mechanical treatment, an observer at the center of a converging gradient would be situated at the central antinode of a spherical Bessel function. This geometry suggests that the ”smooth” distribution of matter we assume might actually mask a radial interference pattern.

If this refractive effect holds, one might expect to observe subtle, concentric modulations in the density or luminosity of large-scale structures centered on the observer: effectively a cosmic ”bullseye” of constructive and destructive interference zones. While currently attributed to Baryon Acoustic Oscillations (BAO) or selection biases, these concentric shells of matter (e.g., the ”Great Walls”) could physically correspond to the nodal structure of the vacuum's refractive index. This perspective offers a novel geometric unification: the ”quantization” of large-scale structure may be an optical artifact of our position at the center of a refractive potential well.

7 Conclusion

We have presented the **Cosmological Lensing Effect** as a geometric correction to the standard cosmological framework. By treating the large-scale density gradient as a refractive medium, we recover the observational signatures of expansion and acceleration without invoking dark energy.

Quantitative analysis using a constrained NFW profile against the Pantheon+ dataset demonstrates that the results are statistically robust. A joint likelihood analysis yields a best-fit background expansion of $H_0 = 67.53 \pm 0.01$ km s^{-1} Mpc^{-1} and a refractive scale radius of $r_s \approx 830$ Mpc, which physically aligns with the scale of the local supercluster basin. Furthermore, the implied mass budget converges to $\sim 10^{76}$ protons, consistent with the baryonic mass of the observable structure, effectively removing the requirement for dark matter in the local volume.

Crucially, this framework distinguishes itself from prior inhomogeneous models by strictly preserving the **shear-free condition** of the background light bundle. Because the effect is refractive rather than kinematic, it potentially satisfies the stringent isotropy constraints of the CMB while simultaneously resolving the local Hubble Tension.

By decoupling the age of the universe from the local Hubble gradient, this model naturally resolves the ”Impossible Galaxy” paradox observed by JWST. We conclude that the ”Hubble Tension” may not be a crisis of cosmology, but rather the refractive signature of a global density gradient - a geometric reality that unifies the local and global universe under a single, baryon-consistent potential.

A Geometry of the Local Potential

To visualize the physical implication of the measured scale radius ($r_s \approx 830$ Mpc), we compare the effective refractive potential profile $\phi(z)$ for the measured median against a larger, flatter hypothesis ($r_s = 2000$ Mpc).

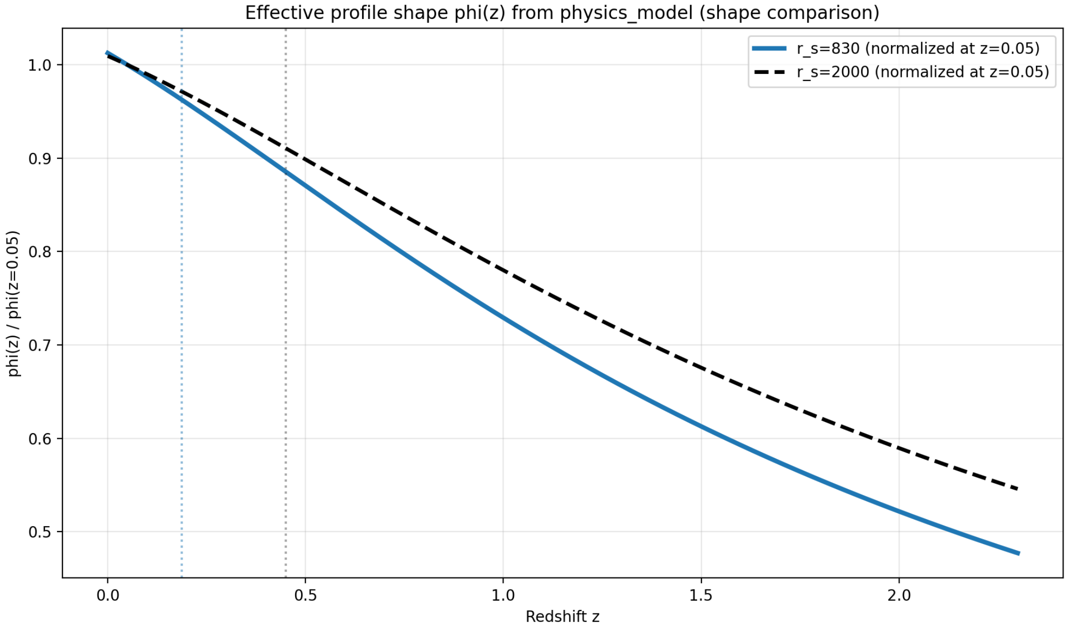

Figure 3: **The "Teardrop" Geometry of the Local Potential.** Comparison of the normalized refractive profile $\phi(z)$ for the measured median $r_s = 830$ Mpc (solid blue) versus a larger scale $r_s = 2000$ Mpc (dashed black). The $r_s = 830$ Mpc profile exhibits a sharper "knee" at low redshift ($z \approx 0.2$), characteristic of a "Teardrop" geometry. This transition corresponds to a lookback time of ≈ 2.5 Gyr, marking the temporal boundary of the coherent density basin associated with the Local Supercluster assembly.

References

[1] Alcock, C., & Paczynski, B. (1979). An evolution free test for non-zero cosmological constant. *Nature*, 281, 358–359.

[2] Bondi, H. (1947). Spherically symmetrical models in general relativity. *Monthly Notices of the Royal Astronomical Society*, 107(5-6), 410-425.

[3] Brout, D., et al. (2022). The Pantheon+ Analysis: Cosmological Constraints from the Combined Pantheon+ and SH0ES Supernova Samples. *The Astrophysical Journal*, 938(2), 110.

[4] Luongo, O., Muccino, M., Ó Colgáin, E., Sheikh-Jabbari, M. M., & Yin, L. (2022). On Larger H_0 Values in the CMB Dipole Direction. *Physical Review D*, 105(10), 103510.

[5] Di Valentino, E., Melchiorri, A., & Silk, J. (2019). Planck evidence for a closed Universe and a possible crisis for cosmology. *Nature Astronomy*, 4, 196–203.

[6] Di Valentino, E., Melchiorri, A., & Silk, J. (2020). Cosmic discordance: Planck and luminosity distance data exclude LCDM. *Astroparticle Physics*, 114, 102351.

[7] Di Valentino, E., ... Vagnozzi, S., et al. (2021). In the realm of the Hubble tension—a review of solutions. *Classical and Quantum Gravity*, 38(15), 153001.

[8] Durrer, R. (2008). *The Cosmic Microwave Background.* Cambridge University Press.

[9] Durrer, R. (2011). What do we really know about Dark Energy? *Philosophical Transactions of the Royal Society A*, 369, 5102-5114.

[10] Efstathiou, G. (2021). To H0 or not to H0?. *Monthly Notices of the Royal Astronomical Society*, 505(3), 3866-3872.

[11] Evans, J., Alsing, P. M., Giorgetti, S., & Nandi, K. K. (2001). Matter waves in a gravitational field: An index of refraction for massive particles in general relativity. *American Journal of Physics*, 69(10), 1103-1110.

[12] Holanda, R. F. L., Lima, J. A. S., & Ribeiro, M. B. (2012). Probing the Cosmic Distance Duality Relation with the Sunyaev-Zel'dovich Effect, X-rays Observations and Supernovae Ia. *Astronomy & Astrophysics*, 538, A131.

[13] Holanda, R. F. L., et al. (2019). Galaxy cluster Sunyaev-Zel'dovich effect scaling-relation and type Ia supernova observations as a test for the cosmic distance duality relation. *Journal of Cosmology and Astroparticle Physics*, 2019(06), 008.

[14] Jackson, J. D. (1999). *Classical Electrodynamics* (3rd ed.). Wiley.

[15] Kalbouneh, A., et al. (2025). Bulk Flow of the Local Universe: A Spherical Analysis. *arXiv preprint*, arXiv:2510.02510.

[16] Kaplan, L., et al. (2020). Observation of branched flow of light. *Nature*, 583, 35–39.

[17] Labbé, I., et al. (2023). A population of red candidate massive galaxies ∼600 Myr after the Big Bang. *Nature*, 616, 266–269.

[18] Landau, L. D., & Lifshitz, E. M. (1975). *The Classical Theory of Fields* (Vol. 2). Elsevier. (Specifically Section 88, regarding Fermat's Principle in a static gravitational field).

[19] Lemaître, G. (1933). The expanding universe. *Annales de la Société Scientifique de Bruxelles*, A53, 51.

[20] Minami, Y., & Komatsu, E. (2020). New Extraction of the Cosmic Birefringence from the Planck 2018 Polarization Data. *Physical Review Letters*, 125(22), 221301.

[21] Navarro, J. F., Frenk, C. S., & White, S. D. M. (1996). The Structure of Cold Dark Matter Halos. *The Astrophysical Journal*, 462, 563.

[22] Peterson, E. R., et al. (2022). The Pantheon+ Analysis: Evaluating Peculiar Velocity Corrections in Cosmological Analyses with Nearby Type Ia Supernovae. *The Astrophysical Journal*, 938(2), 112.

[23] Planck Collaboration. (2016). Planck 2015 results. XXVII. The Sunyaev-Zeldovich cluster catalogue. *Astronomy & Astrophysics*, 594, A27.

[24] Riess, A. G., et al. (1998). Observational Evidence from Supernovae for an Accelerating Universe and a Cosmological Constant. *The Astronomical Journal*, 116(3), 1009.

[25] Schneider, P., Ehlers, J., & Falco, E. E. (1992). *Gravitational Lenses.* Springer-Verlag Berlin Heidelberg.

[26] Scolnic, D., et al. (2022). The Pantheon+ Analysis: The Full Data Release. *The Astrophysical Journal*, 938(2), 113.

[27] Secrest, N. J., et al. (2021). A Test of the Cosmological Principle with Quasars and the Cosmic Microwave Background. *The Astrophysical Journal Letters*, 908(2), L51.

[28] White, R. M. T., et al. (2024). The Dark Energy Survey Supernova Program: Slow supernovae show cosmological time dilation out to $z \approx 1$. *arXiv preprint*, arXiv:2406.05050.

[29] Wiltshire, D. L. (2007). Cosmic clocks, cosmic variance and cosmic averages. *New Journal of Physics*, 9(10), 377.

[30] Wiltshire, D. L. (2009). Average observational quantities in the timescape cosmology. *Physical Review D*, 80(12), 123512.

[31] Ye, X. H., & Lin, Q. (2008). Gravitational lensing analyzed by the graded refractive index of a vacuum. *Journal of Optics A: Pure and Applied Optics*, 10(7), 075001.

[32] Zhang, P., & Stebbins, A. (2011). Confirmation of the Copernican Principle at Gpc Scales. *Physical Review Letters*, 107(4), 041301.

[33] Gordon, W. (1923). Zur Lichtfortpflanzung nach der Relativitätstheorie. *Annalen der Physik*, 377(22), 421-456.